JCIM JOURNAL OF CHEMICAL INFORMATION AND MODELING

pubs.acs.org/jcim Article

Lipid Oxidation: Role of Membrane Phase-Separated Domains

Maria C. Oliveira, Maksudbek Yusupov, Annemie Bogaerts, and Rodrigo M. Cordeiro*

Cite This: J. Chem. Inf. Model. 2021, 61, 2857−2868 Read Online

ACCESS | Metrics & More | Article Recommendations | Supporting Information

ABSTRACT: Lipid oxidation is associated with several inflammatory and neurodegenerative diseases, but many questions to unravel its effects on biomembranes are still open due to the complexity of the topic. For instance, recent studies indicated that phase-separated domains can have a significant effect on membrane function. It is reported that domain interfaces are "hot spots" for pore formation, but the underlying mechanisms and the effect of oxidation-induced phase separation on membranes remain elusive. Thus, to evaluate the permeability of the membrane coexisting of liquid-ordered (Lo) and liquid-disordered (Ld) domains, we performed atomistic molecular dynamics simulations. Specifically, we studied the membrane permeability of nonoxidized or oxidized homogeneous membranes (single-phase) and at the Lo/Ld domain interfaces of heterogeneous membranes, where the Ld domain is composed of either oxidized or nonoxidized lipids. Our simulation results reveal that the addition of only 1.5% of lipid aldehyde molecules at the Lo/Ld domain interfaces of heterogeneous membranes increases the membrane permeability, whereas their addition at homogeneous membranes does not have any effect. This study is of interest for a better understanding of cancer treatment methods based on oxidative stress (causing among others lipid oxidation), such as plasma medicine and photodynamic therapy.

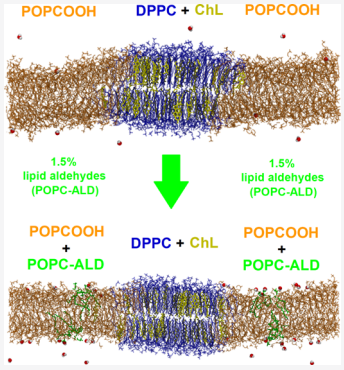

INTRODUCTION

The major structural lipids in eukaryotic membranes are the phospholipids. They have a nearly cylindrical molecular geometry composed of saturated and cis-unsaturated fatty acid chains, which render them fluid at room temperature.[1] These fatty acid chains can be oxidized by specific enzymes[2] or free radicals, namely reactive oxygen and nitrogen species (RONS).[3] The oxidative attack by free radicals may lead to oxidative stress situations in the fatty acid chains, generating relatively stable products bearing functional groups, such as hydroperoxide, hydroxyl, and truncated acyl chains with aldehyde and carboxylic groups.[4,5] These oxidized lipids affect the microscopic and macroscopic properties of the membrane, which may be associated with several inflammatory, cancer, and neurodegenerative diseases.[6−8]

Lipids and proteins can diffuse laterally in the membrane, creating a random mosaic-like structure that has the fluidity of vegetable oil.[9] Despite the latter, there is a large body of experimental evidence suggesting that, rather than being randomly distributed, lipids and proteins are able to organize in nanodomains, enriched in cholesterols and saturated sphingolipids, revealing a lipid heterogeneity in the membrane.[10,11] These domains are referred to as "lipid rafts" and serve as rafts for the transport of selected molecules[12] or as relay stations in intracellular signaling.[13,14] Changes in raft sizes can affect the function of the plasma membrane, for example, by altering the capacity of membrane domains to accommodate proteins that must interact for signaling. Several experimental works have demonstrated the heterogeneity in biomembranes.[15−17] However, there are many technical challenges associated with the observation of nanometer-scale changes in lipid composition.[18,19]

The surface of any living cell, either prokaryotic or eukaryotic, is a complex assembly of a variety of molecular components comprising lipids and embedded proteins. It is supported by the cytoskeletal meshwork attached to the plasma membrane via anchoring proteins. Arumugam and co-workers demonstrated that the interaction of transmembrane or membrane binding proteins with the cytoskeleton maintains the heterogeneity (phase separation) of the plasma membrane, even above the transition temperature.[20]

Lipid rafts form distinct liquid-ordered (Lo) phase-separated domains in the lipid bilayer, dispersed in a liquid-disordered (Ld) matrix of unsaturated lipids, which might play a significant role in the plasma membrane of living cells.[21,22] In addition, lipid oxidation may induce Lo/Ld phase separation in membranes.[23] Tsubone and co-workers proposed that the lipid hydroperoxide, an oxidized lipid with cylindrical molecular geometry,[24] is a promoter of Lo/Ld phase separation, whereas the lipid carboxylic acid, which has a conical molecular geometry, does not cause phase separation, but directly influences the bilayer deformation and membrane leakage.[25] Thus, oxidation-induced

Received: January 31, 2021
Published: June 3, 2021

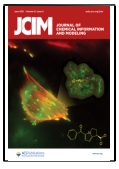

https://doi.org/10.1021/acs.jcim.1c00104
J. Chem. Inf. Model. 2021, 61, 2857−2868

phase separation might have serious consequences for cell membranes that are subject to oxidative stress.

The fluidity of a lipid bilayer is affected by the hydration level, temperature, lipid composition, and cholesterol content of the membrane. At low temperature, the lipid tails can pack closely together to form a crystalline lamellar subgel phase (Lc), with hydrocarbon chains untilted with respect to the bilayer normal, and the long axis of the headgroup oriented parallel to the bilayer normal. Upon heating, the Lc phase undergoes a subtransition to a lamellar gel phase less ordered than the Lc phase, with untilted chains (Lβ) (fairly rigid) or tilted chains (Lβ') (less rigid). The addition of cholesterol transforms the gel phase into a Lo phase. At higher temperatures, i.e., during the so-called pretransition, an interconversion between two different gel phases takes place: the Lβ' phase transforms into a periodic modulation called the rippled gel phase (Pβ'). Upon further heating, the Pβ' phase undergoes a highly cooperative transition to a lamellar liquid crystalline phase (Lα) that is more fluid[26,27] (Figure 1).

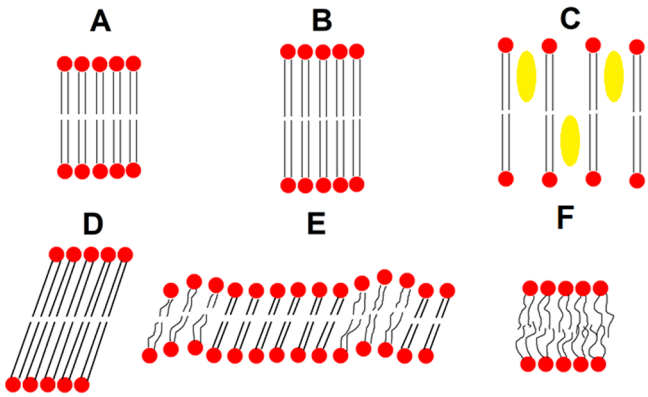

Figure 1. Schematic representation of the various lamellar lipid phases: (A) crystalline lamellar subgel (Lc); (B) gel with untilted chains (Lβ); (C) liquid-ordered (Lo), where the filled oval circles in yellow represent cholesterol molecules; (D) gel with tilted chains (Lβ'); (E) rippled gel (Pβ'); and (F) liquid crystalline (Lα).

Phase-separated domains (caused by lipid rafts) are very important in membrane research. Theoretical studies suggested that the interfaces between phase-separated domains are regions where pore formation is facilitated. The interface region was roughly 2−4 orders of magnitude more permeable to Na^+ ions than the fluid phase.[28] However, for the membrane as a whole to be leaky, it needs to be strongly microheterogeneous with a large number of interfacial regions. That is why membranes become leaky near the gel−fluid transition temperature: many interfacial regions develop since the quasi-critical transition regime is approached.[29−31] Ghysels and co-workers studied the permeation of oxygen and water molecules through membranes with Lo and Ld phases using molecular dynamics (MD) simulations and electron paramagnetic resonance (EPR) spectroscopy. They demonstrated that the oxygen and water molecules enter through the Lo phase, diffuse laterally in the membrane core, and then leave the membrane along the boundary regions.[32] Nevertheless, the interfacial permeability is still not fully understood, being a challenge both experimentally and in computer simulations.

It is well-known that lipid oxidation products affect the microscopic and macroscopic properties of the membrane, inducing structural and conformational changes related to the area per lipid, lipid order, bilayer thickness,[33] and bilayer hydration profile.[34] These changes might in turn induce pore formation and thus affect the membrane permeability. Recently, we showed that nitrated lipids (also produced by free radicals) considerably increase the membrane permeability.[35] Boonnoy and co-workers observed the formation of water defects induced by both lipid aldehydes and lipid hydroperoxides, where full pore formation was observed only in the bilayer consisting of lipid aldehydes. At 50% oxidation with lipid aldehydes, the pores were stable. However, at higher concentrations, the pores became unstable and micellation occurred within 1 μs.[36]

Van der Paal and co-workers showed that the membrane permeability may be influenced by different lipid molecules present in the membrane. For instance, the presence of both aldehyde fragments (produced as a result of lipid chain break) and cholesterol were shown to reduce the susceptibility of membranes to pore formation.[37] Thus, it can be expected that other oxidized lipids formed in the membrane may modulate the permeabilization effect of lipid aldehydes. In this study, we investigate the role of lipid oxidation on the permeability of phase-separated domains, using MD simulations. We hope that our study contributes to a better understanding of the effects of products generated during photosensitized reactions used in photodynamic therapies,[38] as well as during lipid oxidation caused by plasma medicine.[39,40]

METHODS

We performed MD simulations using the software GROMACS version 5.1.2,[41] applying the united-atom GROMOS 53A6 force field.[42] We used well-validated models for the description of unsaturated lipids[43] and lipid hydroperoxides.[44] We adopted interatomic interaction parameters for the aldehyde functional groups from the standard GROMOS 53A6 force field library.[42,45] This force field reproduces very well experimental data from biomolecules in general,[46] and specifically from biomembranes.[43]

In our simulations, we used heterogeneous model membranes composed of POPC (1-palmitoyl-2-oleoyl-*sn*-glycero-3-phosphocholine) molecules and their oxidation products that contain hydroperoxide (POPCOOH) and aldehyde (POPC-ALD) functional groups. The hydroperoxide group was added with *R* stereocenter at C9 carbon (see Figure 2). All initial systems were built using the Packmol software,[47] and graphical renderings were produced using the VMD software version 1.9.3.[48]

MD Protocol. We started the simulations from a membrane with preformed domains with assumed compositions, consistent with either the Lo or Ld phases. Each system was composed of coexisting Lo and Ld domains: one consisting of DPPC (1,2-dipalmitoyl-phosphatidylcholine) + cholesterol (ChL) molecules (Lo phase) and another consisting of native POPC or POPCOOH (Ld phase). Earlier simulations have suggested the formation of a constriction region (i.e., a region with minimal membrane thickness) at the gel/fluid interface, which could also enhance membrane permeability.[28] Thus, we added POPC-ALD lipid molecules to the Lo/Ld domain interface region of our model membranes, because it is the region where they might elicit the strongest effect. These systems were then covered with water molecules on top and at the bottom. The structure of each lipid, as well as cholesterol, used in our simulations can be seen in Figure 2. They are representative of typical products of lipid oxidation.[3,49]

Water molecules were modeled with the simple point charge (SPC) model.[50] Periodic boundary conditions were used in all Cartesian directions. Newton's equations of motion were

https://doi.org/10.1021/acs.jcim.1c00104
J. Chem. Inf. Model. 2021, 61, 2857−2868

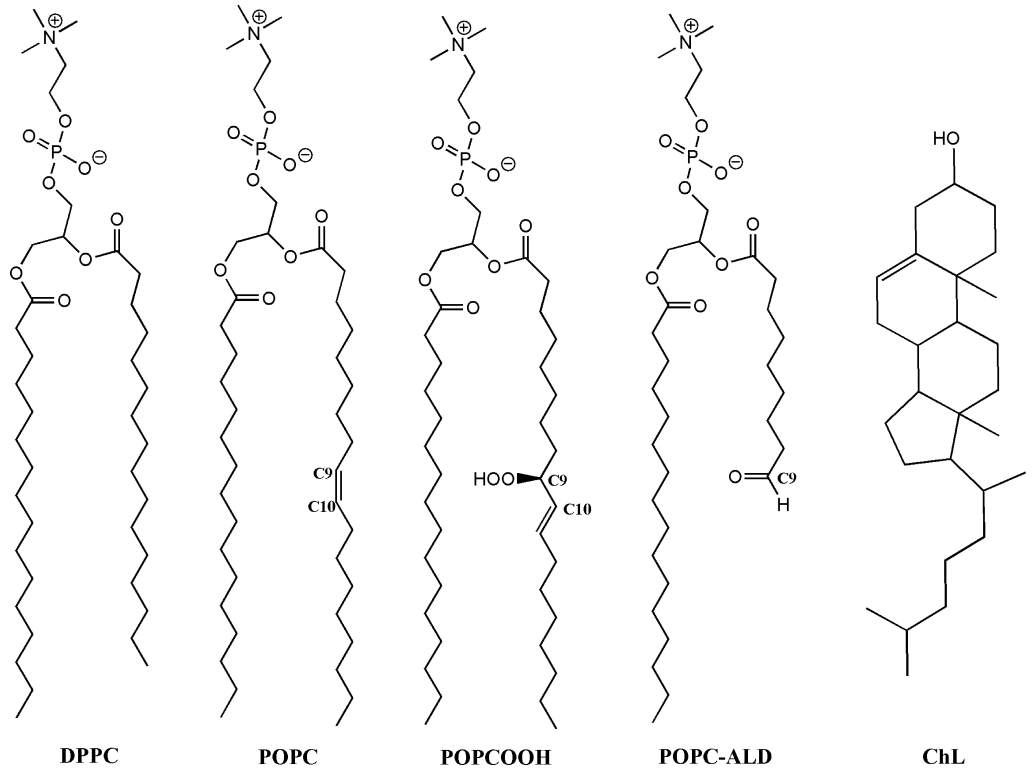

Figure 2. Structure of each lipid and cholesterol (ChL) molecules used in our simulations. See the text for the full names.

Table 1. Composition of Each Simulated Membrane[a]

	number of molecules						
		native lipids		oxidized lipids			
system	ChL	DPPC	POPC	POPCOOH	POPC-ALD	water	box dimensions (nm)
DPPC + ChL/POPC	54	128	256			17524	18.74, 6.30, 8.75
DPPC + ChL/POPC + 6 POPC-ALD	54	128	244		12	17523	19.26, 6.09, 8.81
DPPC + ChL/POPC + 32 POPC-ALD	54	128	192		64	17523	19.26, 6.09, 8.81
DPPC + ChL/POPCOOH	54	128		256		17524	19.58, 6.35, 8.34
DPPC + ChL/POPCOOH + 6 POPC-ALD	54	128		244	12	17524	23.64, 5.69, 7.69
DPPC + ChL/POPCOOH + 16 POPC-ALD	54	128		224	32	17524	21.04, 6.08, 8.11
DPPC + ChL/POPCOOH + 32 POPC-ALD	54	128		192	64	17523	19.83, 6.06, 8.52

[a]The number of POPC and oxidized lipids corresponds to the total lipids in the two membrane domains.

integrated using the leapfrog algorithm with a time step of 2 fs. A cutoff radius of 1.4 nm was used for nonbonded (Lennard-Jones) interactions. Coulomb interactions were treated using the PME method. The covalent bond lengths were constrained using the LINCS algorithm.

We performed a steepest descent energy minimization, followed by equilibration at the NPT ensemble for at least 300 ns. The temperature was maintained close to the physiological temperature (310 K) by coupling the system to an external temperature bath using the Nose−Hoover thermostat.[51,52] The temperature coupling constant was 0.5 ps. The pressure was also maintained at around 1 bar by coupling the system to an external pressure bath using the Parrinello−Rahman barostat.[53] The pressure coupling was applied semi-isotropically with a coupling constant of 2 ps and isothermal compressibility of 4.5×10^{-5} bar^{-1}.[54] Note that the chosen equilibration time (300 ns) was sufficient, as the membrane areas of all systems converged within this time (see Figure S1 in the Supporting Information (SI)).

Data Analysis. All membrane properties were calculated from the last 100 ns of the simulation. The area per lipid of each domain was calculated by Voronoi tessellations implemented in the voro++ software.[55] The area per lipid was calculated using a set of key atoms in the Voronoi analysis. For lipids, both carbonyl carbons and the CH_1 group in the glycerol moiety were used as key atoms. For cholesterol, the oxygen atom of the hydroxyl group was used. The bilayer thickness was calculated using the gmx traj tool of the GROMACS program. It was defined as the average distance along the z-axis between the center of mass of the phosphorus atoms of both leaflets. The uncertainties were calculated by standard deviation of the average values.

The distribution of the curvature order parameter was calculated using the s_order program of the software Surface Assessment via Grid Evaluation (SuAVE),[56] with a mesh resolution of 40 401 and corresponding bin values of 200. This program calculates the average curvature order parameter distribution $P(\theta)$ of the angles θ between the z-axis and the

https://doi.org/10.1021/acs.jcim.1c00104
J. Chem. Inf. Model. 2021, 61, 2857−2868

normal vectors of the surface rectangular grid partitions, over all trajectory frames:

$$P(\theta) = \frac{1}{2}(3\cos^2(\theta) - 1) \quad (1)$$

The curvature order parameter ranges from $P(90°) = -0.5$ to $P(0°) = 1$. In the first case, the normal vector of the surface is perpendicular to the z-axis (larger curvatures). In the second case, the normal vector of the surface is parallel (smaller curvatures). The software for calculation of the number of water molecules crossing the membrane was developed by the research group of Prof. Alexandre Suman de Araujo, from IBILCE/UNESP.[57] The numbers of permeation events were calculated using a single model membrane, except for the POPCOOH + 6 POPC-ALD and DPPC + ChL/POPCOOH + 6 POPC-ALD, where three replicates were used for averaging.

RESULTS AND DISCUSSION

We performed MD simulations for model membranes composed of two coexisting domains: the Lo domain was composed of DPPC + ChL molecules and the Ld domain was composed of either POPC or POPCOOH lipids. We also performed MD simulations by adding different quantities of POPC-ALD lipid molecules to the Lo/Ld domain interface regions of the membranes. The compositions of our model systems are given in Table 1 (and see also Figures 3 and 4).

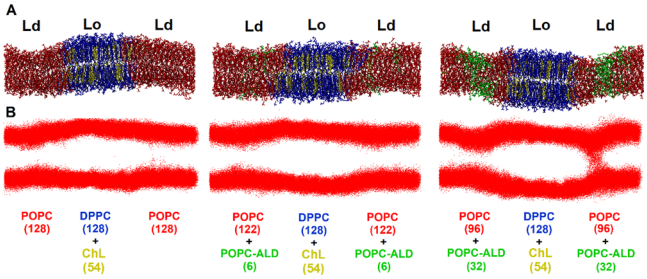

Figure 3. (A) Snapshots of heterogeneous membranes at 300 ns of simulation, where the Ld phase is composed of POPC lipid molecules. (B) Trajectories of water molecules. Lipid molecules were removed for clarity, and water molecules are represented as red points. All frames of the last 100 ns were overlaid in order to highlight the permeation path of water molecules.

Membrane Structural Properties. Note that our simulations reveal a thickness mismatch between different phases, i.e., the thickness of the Lo domain was larger than that of the Ld domain (Figures 3A and 4A). In line with previous studies of the gel/fluid coexistence,[28] the thickness did not decrease monotonically from the Lo to the Ld phase. Instead, a thickness minimum (i.e., a constriction region) is formed at the Lo/Ld interface (Figure 5), due to the elastic deformation of the Ld domain in the region near to the domain interface.

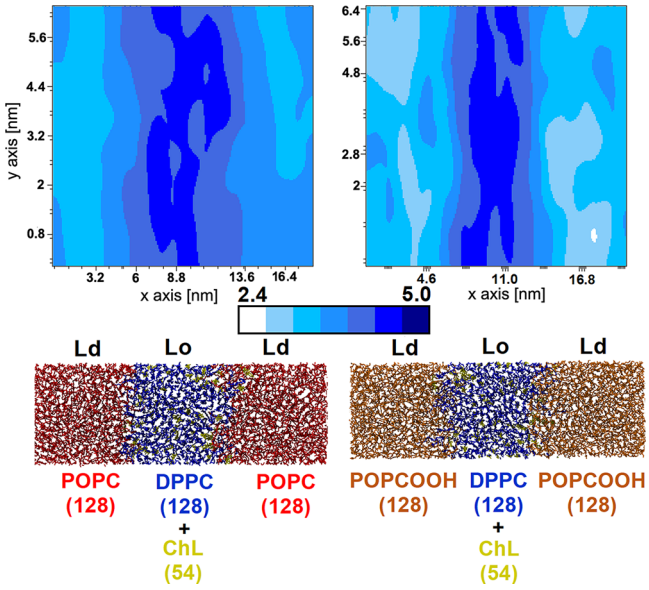

Figure 5. Two-dimensional frame-averaged distribution of the bilayer thickness calculated from the last 100 ns of simulation. The mesh resolution is 40 401, and corresponding bin values are equal to 200. These distributions were calculated using the software SuAVE. Both panels represent a top view of the membrane systems. In the upper panel we can see the bilayer thickness of the bottom panel. Box sizes in x and y-axes are the same in the upper and bottom figures, but they are represented in different scales.

By adding POPC-ALD lipid molecules at the Lo/Ld domain interfaces, we observed more water molecules crossing the membrane through this region. The effect was more pronounced in the POPC (Figure 3B) than in the POPCOOH domain (Figure 4B). We witnessed stronger undulations and membrane bending in the case of POPCOOH (cf. Figures 3A and 4A), which can be the reason for the lower permeability of the POPCOOH domain. For the DPPC + ChL/POPCOOH + 16 POPC-ALD system, the permeation was similar to that of the

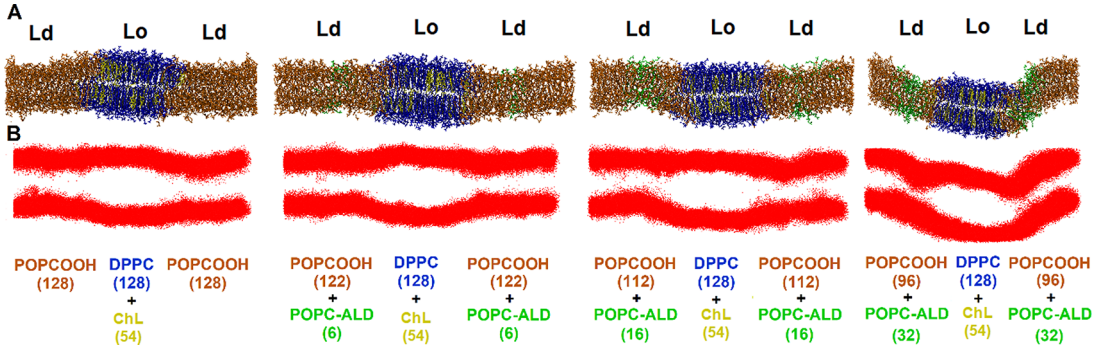

Figure 4. (A) Snapshots of heterogeneous membranes at 300 ns of simulation, where the Ld phase is composed of POPCOOH lipid molecules. (B) Trajectories of water molecules. Lipid molecules were removed for clarity, and water molecules are represented as red points. All frames of the last 100 ns were overlaid in order to highlight the permeation path of water molecules.

https://doi.org/10.1021/acs.jcim.1c00104
J. Chem. Inf. Model. 2021, 61, 2857−2868

Table 2. Area per Lipid and Bilayer Thickness of All Model Membranes Simulated[a]

	area per lipid (nm^2) and bilayer thickness (nm)				
		native lipids		oxidized lipids	
system	ChL	DPPC	POPC	POPCOOH	POPC-ALD
DPPC + ChL/POPC	0.18 ± 0.06	0.59 ± 0.19	0.58 ± 0.19		
		(4.54 ± 0.03)	(3.81 ± 0.03)		
DPPC + ChL/POPC + 6 POPC-ALD	0.20 ± 0.06	0.59 ± 0.19	0.58 ± 0.19		0.60 ± 0.19
		(4.44 ± 0.07)	(3.83 ± 0.06)		(3.61 ± 0.16)
DPPC + ChL/POPC + 32 POPC-ALD	0.20 ± 0.07	0.59 ± 0.19	0.58 ± 0.22		0.59 ± 0.20
		(4.52 ± 0.04)	(3.70 ± 0.04)		(2.97 ± 0.09)
DPPC + ChL/POPCOOH	0.21 ± 0.08	0.64 ± 0.24		0.62 ± 0.23	
		(4.36 ± 0.04)		(3.43 ± 0.03)	
DPPC + ChL/POPCOOH + 6 POPC-ALD	0.22 ± 0.08	0.66 ± 0.26		0.66 ± 0.26	0.71 ± 0.28
		(4.47 ± 0.03)		(3.22 ± 0.03)	(3.03 ± 0.13)
DPPC + ChL/POPCOOH + 16 POPC-ALD	0.22 ± 0.09	0.65 ± 0.25		0.62 ± 0.26	0.63 ± 0.26
		(4.37 ± 0.04)		(3.32 ± 0.03)	(3.29 ± 0.09)
DPPC + ChL/POPCOOH + 32 POPC-ALD	0.20 ± 0.13	0.59 ± 0.49		0.60 ± 0.42	0.61 ± 0.60
		(4.32 ± 0.11)		(3.50 ± 0.09)	(3.10 ± 0.07)

[a]The bilayer thickness is represented between brackets.

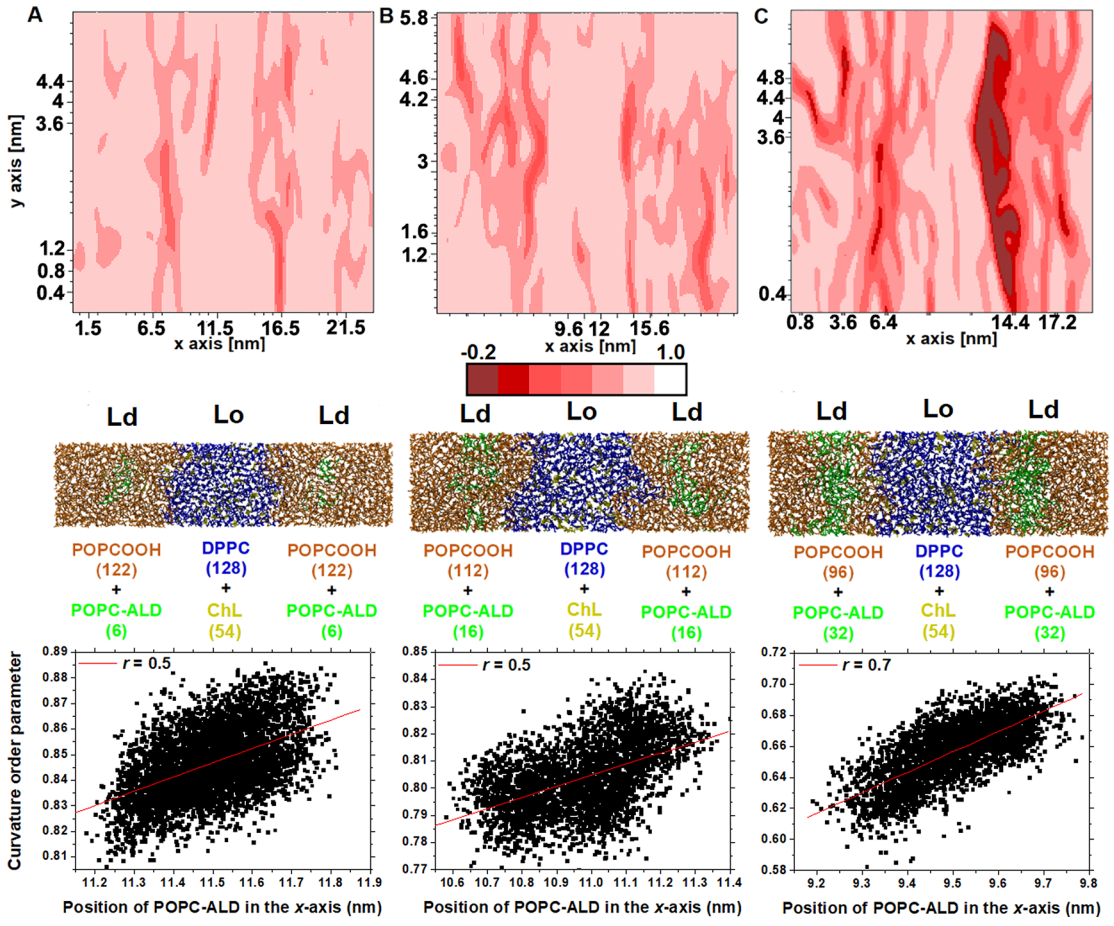

Figure 6. Two-dimensional frame-averaged distribution of the curvature order parameter calculated from the last 100 ns of simulation, for the different systems. These distributions were calculated using the software SuAVE. Both panels represent a top view of the membrane systems. In the upper panel we can see the membrane curvature of the bottom panel. It should be noted that the upper graphs and bottom snapshots are not in the same scale. The bottom-most graphs represent the Pearson correlation coefficient (r) of the curvature order parameter vs position of POPC-ALD lipids.

DPPC + ChL/POPCOOH + 6 POPC-ALD system. Note that the increase in the membrane permeability is more visible when we have a lot of POPC-ALD molecules at the Lo/Ld domain interfaces. In order to determine the effect caused by few POPC-ALD molecules, we will calculate the number of water molecules crossing the membrane (see the section Membrane Permeability). Note that the Lo/Ld domain interface region consists of a constriction region together with the gel/fluid interface (see the red rectangle in Figure S2).

https://doi.org/10.1021/acs.jcim.1c00104
J. Chem. Inf. Model. 2021, 61, 2857−2868

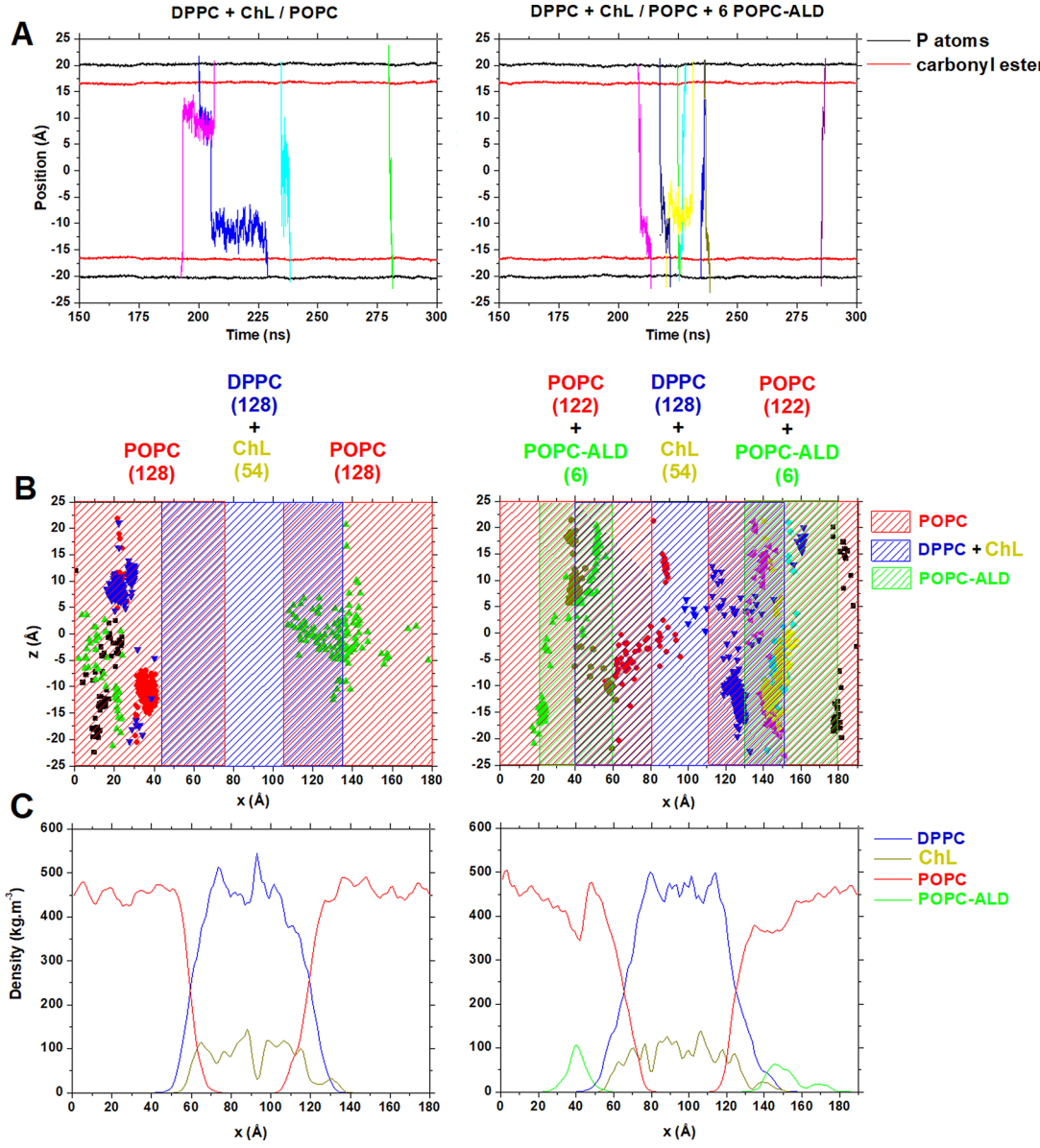

Figure 7. (A) Number of water permeation events calculated from the last 150 ns of simulation to measure the effect caused by addition of POPC-ALD lipid molecules at POPC domains. Each line color represents only one permeation event. (B) Two-dimensional distribution of water permeation events over the last 150 ns of simulation. Each symbol with specific color represents only one permeation event. (C) Density profile along the *x*-axis calculated from the last 150 ns of simulation.

Experimental measurements from the literature revealed a 10-fold increase in membrane permeability upon addition of minute amounts (2.5%) of lipid aldehydes.[58] However, molecular simulations showed the formation of membrane poration (which is a measure for membrane permeability) only at aldehyde molar fractions larger than 50%.[36] We conjectured that (i) depending on composition or external effects such as oxidation, membranes might become microheterogeneous at the nanoscopic scale; (ii) short-chain aldehydes that are formed along other oxidation products might have a preference for the constriction region at the domain boundaries, where they would concentrate and elicit a stronger permeabilization effect. Lipid lateral diffusion involves time scales that are difficult to achieve in atomistic simulations. Many studies of the membrane phase behavior were conducted with lower-resolution coarse-grained models.[59,60] Here, we pursued a simplified, yet meaningful, strategy in which we assumed an enhanced aldehyde concentration at the interface and checked whether it would contribute to membrane permeabilization.

Area per Lipid and Bilayer Thickness. Table 2 show the areas per lipid and membrane thicknesses recorded for all studied systems. When no POPC-ALD lipid molecules were included, the area per lipid of the POPC domain was 0.58 ± 0.19 nm^2. Within the uncertainty this compares well with the experimental values of 0.64 ± 0.01 and 0.67 ± 0.01 nm^2 obtained for native POPC at 303 and 323 K, respectively, from X-ray scattering.[61] In the case of the POPCOOH domain, the area per lipid was found to be 0.62 ± 0.23 nm^2, hence around 7% higher than that of POPC. The average increase in area per lipid of the POPC system with complete peroxidation was also found in the literature.[62] An increase of the are per lipid reflects the well-known effect of migration of −OOH groups toward the membrane surface.[63,64] The area per DPPC at the Lo domain was 0.59 ± 0.19 nm^2 in the DPPC + ChL/POPC system, and

https://doi.org/10.1021/acs.jcim.1c00104
J. Chem. Inf. Model. 2021, 61, 2857−2868

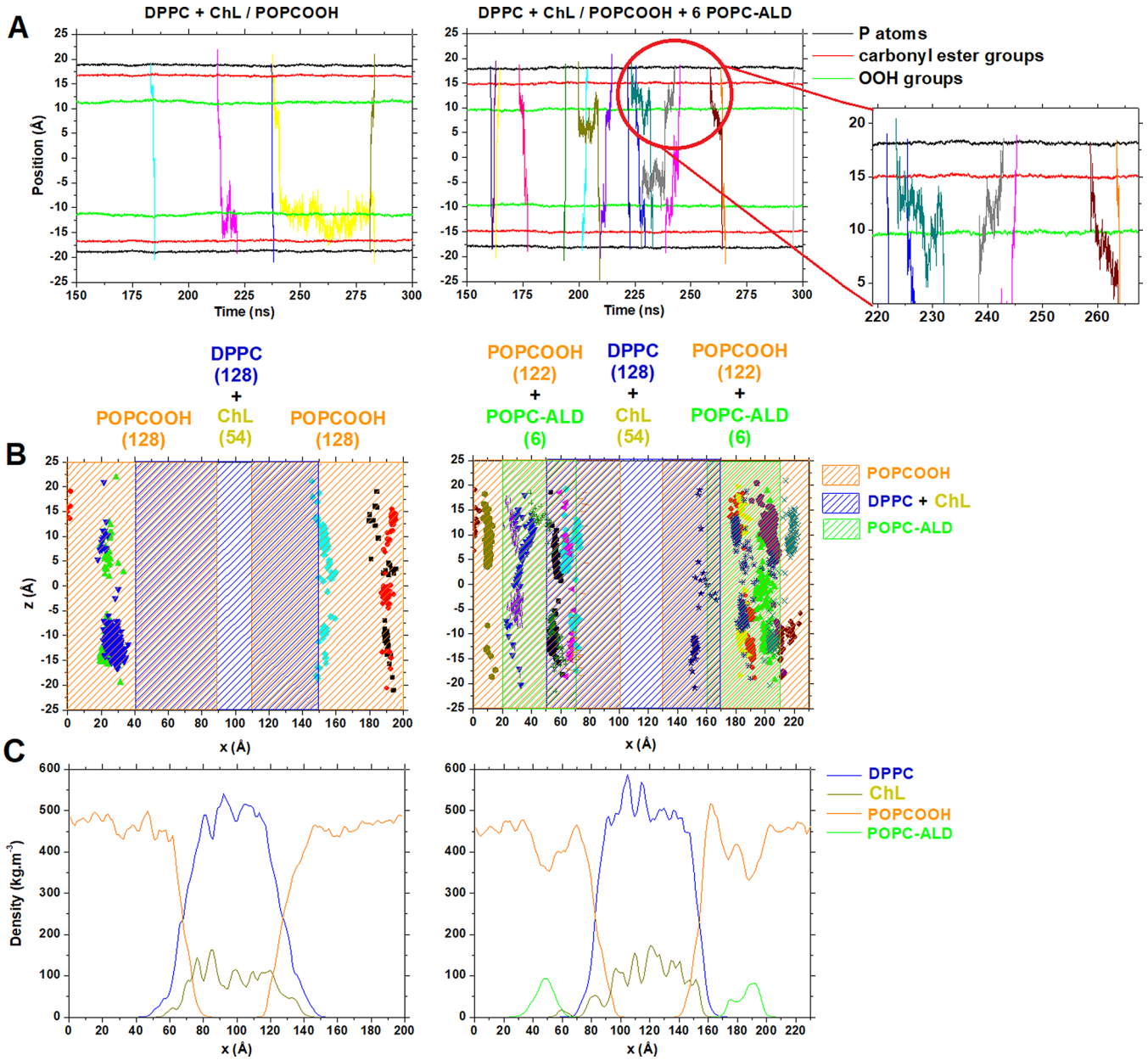

Figure 8. (A) Number of water permeation events calculated from the last 150 ns of simulation to measure the effect caused by addition of POPC-ALD lipid molecules at POPCOOH domains. Each line color represents only one permeation event. Some regions of the graphic on the right side were expanded, in order to show the propensity of the water molecules to spend time at the −OOH groups region. (B) Two-dimensional distribution of water permeation events over the last 150 ns of simulation. Each symbol with specific color represents only one permeation event. (C) Density profile at *x*-axis calculated from the last 150 ns of simulation.

0.64 ± 0.24 nm^2 in the DPPC + ChL/POPCOOH system. The area per ChL in the DPPC + ChL/POPC system was 0.18 ± 0.06 nm^2, whereas it was 0.21 ± 0.08 nm^2 in the DPPC + ChL/POPCOOH system (see Table 2). The bilayer thickness of each domain reveals how much the Ld domain is thinner when compared with the Lo domain (a thickness mismatch). Moreover, the Ld domain is thinner when it is composed of oxidized lipids (see Table 2).

As is clear from Table 2, we obtained relatively large uncertainties in our simulation data. This is due to the fact that the sampling of average values cannot distinguish between lipids at the bulk of the domain and at the interface regions. One of the evidence for this is that the area per lipid of homogeneous membranes (Table S1) had much smaller uncertainties associated. It is in principle possible to calculate the area per lipid locally, but we believe this has limited added value as the results would also be strongly influenced by the strong curvature and undulations at the interfacial region (Figure 4). On the qualitative level, the oxidized systems appeared to have consistently higher values of area per lipid, as expected (Table 2). All model membranes were simulated just a single time, except for the DPPC + ChL/POPCOOH + 6 POPC-ALD system. The latter was simulated in triplicate in order to check for the reproducibility of the results, and all structural properties of the membrane remained equal within the uncertainties (Table S1).

We also calculated the surface curvature order parameter, represented in Figure 6 as two-dimensional frame-averaged

https://doi.org/10.1021/acs.jcim.1c00104
J. Chem. Inf. Model. 2021, 61, 2857−2868

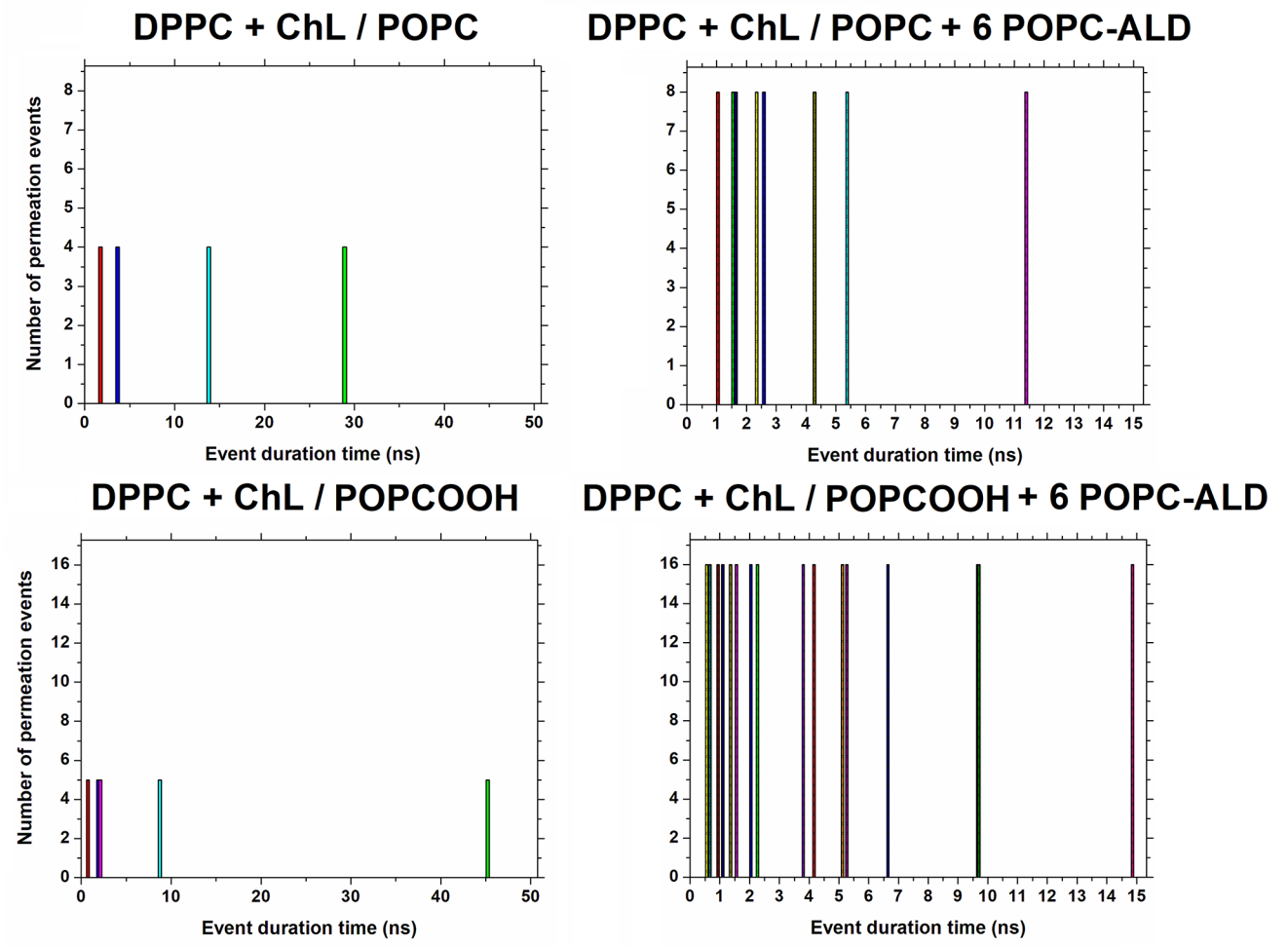

Figure 9. Quantification of the permeation time for the model membranes. Each color bar indicates a duration time of a permeation event. These events were calculated from the last 150 ns of simulation.

distribution. It can help to pinpoint the local positions where the membrane curvature changes, which can be visually correlated to the presence of POPC-ALD lipid molecules. A positive curvature order parameter means that the membrane presents less bending, and a negative value represents more bending.[65] The number of POPC-ALD lipids placed at the domain interfaces is directly related to membrane bending. We can also demonstrate this relation by calculating the Pearson correlation coefficient (r) of the curvature order parameter vs position of POPC-ALD lipids (Figure 6). The Pearson correlation coefficient is a measurement of the strength and association between two variables, i.e., it calculates the effect of changing one variable on the changes in the other variable. The formula of the Pearson correlation coefficient shows the relationship between the variables x and y and yields values between −1 and 1:

$$r = \frac{N\sum xy - [(\sum x)(\sum y)]}{\sqrt{[N\sum x^2 - (\sum x)^2][N\sum y^2 - (\sum y)^2]}} \quad (2)$$

where N is the number of points.

According to Figure 6, we can see a large degree of association between the curvature order parameter and the position of POPC-ALD lipids, with a positive linear relationship, i.e., when the curvature order parameter increases, the position of POPC-ALD lipids also increases. Therefore, the local membrane curvature increases upon adding of POPC-ALD. The membrane surface was concave at the interface, forming an interfacial constriction region with lower thickness. A similar feature has been identified in the literature at the gel/fluid interface of membranes, and it has been shown to lead to a higher tendency for pore formation.[28]

In addition, we calculated the average bilayer thickness (Figure 5 and Table 2). The bilayer thickness of the POPC domain was 3.81 ± 0.03 nm, whereas for the POPCOOH domain it was 3.43 ± 0.03 nm (Table 2), i.e., around 11% lower than for the POPC domain. Because of the thinner bilayer, the POPCOOH domain became more susceptible to membrane fluctuations. The cholesterol molecules largely help to maintain the Lo phase of the DPPC domain: the Lo phase is thicker than the Ld phase (Figure 5). The bilayer thickness of the Lo domain was similar for both systems: 4.54 ± 0.03 and 4.36 ± 0.04 nm in the DPPC + ChL/POPC and DPPC + ChL/POPCOOH systems, respectively (see Table 2). The values of the thickness mismatch between different domains is displayed in Table S2.

Membrane Permeability. As mentioned in previous section, the increase in the membrane permeability can be influenced by many factors, including the presence of oxidized lipids. Furthermore, several studies have demonstrated that by exposing cells to pulsed electric fields (electroporation), it is possible to increase their membrane permeability to ions and various molecules, such as drugs and genes.[66−68] Here, the

https://doi.org/10.1021/acs.jcim.1c00104
J. Chem. Inf. Model. 2021, 61, 2857−2868

membrane permeability was evaluated by following the trajectory of all water molecules that cross the membrane during the last 150 ns of simulation.

Remarkably, when only 6 POPC-ALD lipid molecules were added to each domain interface (i.e., 5% of the lipids of each Ld domain, which corresponds to 1.5% of the total lipids), the membrane permeability doubled. In other words, we counted four permeation events for the DPPC + ChL/POPC system and eight permeation events for the DPPC + ChL/POPC + 6 POPC-ALD system (Figure 7A). Moreover, in the latter system, the water molecules spent less time at the membrane interior compared to the DPPC + ChL/POPC system, meaning that the water molecules diffuse more easily across the membrane in the DPPC + ChL/POPC + 6 POPC-ALD system. This phenomenon is aligned with the fact that the shorter and highly mobile acyl chains of lipid aldehydes are able to act as a water transporter. Interestingly, in the DPPC + ChL/POPC system, most of the permeation events occurred at the bulk of the Ld domain (Figure 7B). This can be correlated with the fluidity of the Ld domain. On the other hand, in the DPPC + ChL/POPC + 6 POPC-ALD system, most of the permeation events occurred both at the domain interfaces (POPC-ALD regions) and at the bulk of the Ld domain (Figure 7B and C).

The addition of 6 POPC-ALD lipid molecules to each of the domain interfaces of the DPPC + ChL/POPCOOH system increases the membrane permeability by a factor of 3: we counted 5 permeation events for the DPPC + ChL/POPCOOH system and 16 ± 3 permeation events for the DPPC + ChL/POPCOOH + 6 POPC-ALD system (see Figures 8A and S3B for DPPC + ChL/POPCOOH + 6 POPC-ALD system replicates). In the absence of POPC-ALD, the permeation events occurred at the bulk of the oxidized domain (Ld domain), while in the presence of POPC-ALD, most of them occurred at the domain interfaces, as well at the bulk of the Ld domain (Figure 8B and C).

Permeation events are all very similar in both systems. Water molecules traverse the headgroup region very rapidly but get stuck for a few ns right below the headgroups region, where they form H-bonds with the carbonyl ester groups. This tendency has already been shown quantitatively in earlier simulation studies.[44] In the case of POPCOOH lipids, the −OOH groups tend to migrate to the headgroup region[62] and then can interact with the water molecules. When water molecules detach from this region, they diffuse across the membrane interior relatively fast. We can see in Figure 9 the duration time (Δt) of the permeation events. Note that in the absence of POPC-ALD lipids we have only a few permeation events. On the other hand, in the presence of POPC-ALD lipids we have much more permeation events with shorter retention time at the carbonyl ester and −OOH groups. Thus, the results suggest a mechanistic picture, according to which the truncated chain of POPC-ALD lipids facilitates water permeation across the interior membrane.

These results suggest that a few lipid aldehydes at the domain interface regions (1.5% of the total lipids) are able to increase the membrane permeability. Wiczew and co-workers showed that a small area of a cell membrane (with or without cholesterol) oxidized with lipid aldehydes, would induce the formation of wide enough pores (up to ∼5 nm diameter) to transport ions and large molecules.[69] Moreover, they showed that the membrane fluidity and the location of the "oxidative spots" might significantly affect the pore's lifespan.[69] However, the question arises: is the POPC-ALD-induced permeabilization stronger at the interface between domains or in the bulk of the Ld region? To answer this question, we simulated single-phase membranes with the same number of POPC-ALD molecules randomly distributed. Our aim was to determine whether the presence of a few lipid aldehyde molecules is enough to increase the membrane permeability in homogeneous POPC or POPCOOH membranes without preformed domains.

Our results revealed that the addition of 5% of POPC-ALD lipid molecules to a nonoxidized homogeneous membrane composed of POPC lipid molecules, which represents part of a Ld domain, was not enough to increase the membrane permeability: the permeability remained the same as in the native POPC system (i.e., three permeation events in each system, see Figure S4A). On the other hand, as discussed above, the addition of the same number of POPC-ALD lipid molecules at the POPC domains of heterogeneous (DPPC + ChL/POPC) membrane was able to increase the membrane permeability by a factor of 2 (Figures 7A). The same is true for the addition of POPC-ALD lipid molecules to an oxidized homogeneous membrane composed of POPCOOH lipid molecules. We found 7 permeation events for the POPCOOH system and 3 ± 3 for the POPCOOH + 6 POPC-ALD system (Figure S5A). As mentioned above, to check the reproducibility of the permeation data, the POPCOOH + 6 POPC-ALD system was simulated in triplicate (see Table S1 and Figure S3A). Thus, our results reveal that the presence of a few lipid aldehydes in homogeneous membranes is not enough to increase the membrane permeability, but their presence at the domain interfaces is able to do that.

It should be mentioned that the systems DPPC + ChL/POPCOOH + 6 POPC-ALD and POPCOOH + 6 POPC-ALD were simulated in triplicate, because they represent heterogeneous and homogeneous membranes, respectively. As is clear from Figure S3, the number of permeation events are similar for each replica, particularly in the DPPC + ChL/POPCOOH + 6 POPC-ALD system, which is the main object of this study. In this sense, the permeation results of other single systems should be acceptable.

In summary, our results show that the presence of a few lipid aldehydes at the domain interfaces increases the membrane permeability 2- to 3-fold. This result can be reproduced even at longer simulation time (500 ns, see Figure S6) which does not affect the average permeability. Thus, the chosen simulation time (300 ns) in our study is sufficient to observe the water permeation events. The same is true when elongating the interface region by increasing the number of lipids and water molecules in the y-axis (Figure S7), revealing that the box size simulated herein is large enough and does not influence the above-mentioned permeation results. The same does not occur when the lipid aldehydes are added randomly in homogeneous membranes. The experimental methods that enable the detection of lipid oxidation products in membranes, are able to detect only the average content of oxidized species and hence cannot distinguish between uniform and localized distribution of oxidized lipids.[70−72]

Note that in our simulations we assumed that the lipid aldehydes accumulated at the domain interfaces, rather than at the Ld domain. To confirm our assumption, we performed coarse-grained (CG) MD simulations, with initial random distribution of lipid aldehydes, to evaluate their lateral diffusion, phase separation and the spontaneous partitioning of them between different phases, over a long simulation time (see Figures S8 and S9). We studied model membranes with two different lipid aldehydes, i.e., either derived from POPC lipids

https://doi.org/10.1021/acs.jcim.1c00104
J. Chem. Inf. Model. 2021, 61, 2857−2868

(POPC-ALD) or derived from DIPC (1,2-dilinoleoyl-*sn*-glycero-3-phosphocholine) lipids (DIPC-ALD). Indeed, our CG simulations demonstrated that the POPC-ALD lipids tend to accumulate at the interface between domains (Figures S8 and S10), but the same does not occur for DIPC-ALD lipids, which remain at the Ld phase (Figures S9 and S10).

To understand the above-mentioned effects, future investigations are required, which will help to determine if the interfacial activity is driven by either lipid geometry or interactions between saturated and unsaturated lipid acyl chains of the lipid aldehydes with the Lo and Ld domains. It is noteworthy that CG models have been successfully used for showing interfacial accumulation of certain lipid types,[73] and that such would help to explain why minute amount of lipid aldehyde are able to cause an order-of-magnitude alteration in membrane permeability.[58]

CONCLUSIONS

We presented an atomistic view of how lipid oxidation affects the permeability of phase-separated domains in model membranes, where the Lo domain was composed of DPPC + ChL molecules and the Ld domain was composed of either POPC or POPCOOH lipid molecules. We also evaluated the effect of the addition of lipid aldehydes at the Lo/Ld domain interfaces. Only 5% of lipid aldehydes alone were not enough to increase the membrane permeability when distributed randomly in single-phase membranes. However, their presence at the Lo/Ld domain interfaces (1.5% of the total lipids) was able to increase the permeability by 2- and 3-fold for nonoxidized and oxidized lipids at the Ld domain, respectively. This might help to explain why minute amount of lipid aldehyde at domain interfaces are able to drastically increase the membrane permeability. This study is of interest for photodynamic therapy and plasma medicine for cancer treatment, to understand the effects caused by free radicals in cell membranes.

Data and Software Availability. GROMACS is free software program used to perform MD simulations. The GROMACS package version 5.1.2 can be downloaded at https://manual.gromacs.org/documentation/5.1.2/download.html. Packmol is also free software which creates initial structures for MD simulations by packing molecules in defined regions of space (defined by the user). The user must provide only the coordinates of one molecule of each type, the number of molecules of each type, and the spatial constraints that each type of molecule must satisfy. We provide in the Supporting Information the inputs used to build up our lipid bilayers (ZIP). Packmol can be downloaded at http://m3g.iqm.unicamp.br/packmol/download.shtml. VMD is also free software for displaying, animating, and analyzing large biomolecular systems using 3D graphics. The VMD package version 1.9.3 can be downloaded at https://www.ks.uiuc.edu/Development/Download/download.cgi?PackageName=VMD. SuAVE is also free software to calculate the surface curvature of chemical systems, as well several curvature-dependent properties like area per lipid, density, order parameter, volume per lipid, and so on. These quantities can be represented either as time-dependent or space- and time-averaged projections over topographical (2D) maps. SuAVE can be downloaded at https://www.biomatsite.net/suave-software. The program used to calculate our membrane permeability detects spontaneous permeation events of water molecules through the lipid bilayer, characterizing its crossing time and trajectory at coordinates x, y, and z. This software can be obtained contacting the authors.[57]

ASSOCIATED CONTENT

Supporting Information

The Supporting Information is available free of charge at https://pubs.acs.org/doi/10.1021/acs.jcim.1c00104.

Membrane structural properties (Tables S1 and S2); membrane equilibration (Figure S1); membrane interface (Figure S2); membrane permeation events (Figures S3−S7); CG results (Figures S8−S10) (PDF)

Molecular topology files (.itp) for the atomistic models (DPPC, ChL, POPC, POPCOOH, POPC-ALD) and CG models (DPPC, ChL, DIPC, POPC-ALD, DIPC-ALD); molecular coordinates (.gro) for all systems at 300 ns; inputs (.inp) for Packmol (ZIP)

AUTHOR INFORMATION

Corresponding Author

Rodrigo M. Cordeiro − *Centro de Ciências Naturais e Humanas, Universidade Federal do ABC, 09210-580 Santo André, SP, Brazil;* orcid.org/0000-0001-7763-4886; Email: rodrigo.cordeiro@ufabc.edu.br

Authors

Maria C. Oliveira − *Centro de Ciências Naturais e Humanas, Universidade Federal do ABC, 09210-580 Santo André, SP, Brazil; Research Group PLASMANT, Department of Chemistry, University of Antwerp, B-2610 Antwerp, Belgium;* orcid.org/0000-0003-4311-7906

Maksudbek Yusupov − *Research Group PLASMANT, Department of Chemistry, University of Antwerp, B-2610 Antwerp, Belgium;* orcid.org/0000-0003-4591-858X

Annemie Bogaerts − *Research Group PLASMANT, Department of Chemistry, University of Antwerp, B-2610 Antwerp, Belgium;* orcid.org/0000-0001-9875-6460

Complete contact information is available at: https://pubs.acs.org/10.1021/acs.jcim.1c00104

Notes

The authors declare no competing financial interest.

ACKNOWLEDGMENTS

We thank Universidade Federal do ABC for providing the computational resources needed for completion of this work and CAPES for the scholarship granted. M.Y. acknowledges the Flanders Research Foundation (grant 1200219N) for financial support.

REFERENCES

(1) van Meer, G.; Voelker, D. R.; Feigenson, G. W. Membrane lipids: where they are and how they behave. *Nat. Rev. Mol. Cell Biol.* **2008**, *9*, 112−124.

(2) Maccarrone, M.; Catani, M. V.; Agrò, A. F.; Melino, G. Involvement of 5-lipoxygenase in programmed cell death of cancer cells. *Cell Death Differ.* **1997**, *4*, 396−402.

(3) Frankel, E. N. Chemistry of Free Radical and Singlet Oxidation of Lipids. *Prog. Lipid Res.* **1984**, *23*, 197−221.

(4) Brodnitz, M. H.; Nawar, W. W.; Fagerson, I. S. Autoxidation of Saturated Fatty Acids. I. Initial Products of Autoxidation of Methyl Palmitate. *Lipids* **1968**, *3*, 59−64.

(5) Jurkiewicz, P.; Olzynska, A.; Cwiklik, L.; Conte, E.; Jungwirth, P.; Megli, F. M.; Hof, M. Biophysics of Lipid Bilayers Containing Oxidatively Modified Phospholipids: Insights from Fluorescence and EPR Experiments and from MD Simulations. *Biochim. Biophys. Acta, Biomembr.* **2012**, *1818*, 2388−2402.

(6) Valko, M.; Leibfritz, D.; Moncol, J.; Cronin, M. T. D.; Mazur, M.; Telser, J. Free radicals and Antioxidants in Normal Physiological Functions and Human Disease. *Int. J. Biochem. Cell Biol.* **2007**, *39*, 44−84.
(7) Bradley-Whitman, M. A.; Lovell, M. A. Biomarkers of Lipid Peroxidation in Alzheimer Disease (AD): an update. *Arch. Toxicol.* **2015**, *89*, 1035−1044.
(8) Munir, R.; Lisec, J.; Swinnen, J. V.; Zaidi, N. Lipid Metabolism in Cancer Cells under Metabolic Stress. *Br. J. Cancer* **2019**, *120*, 1090−1098.
(9) Singer, S. J.; Nicolson, G. L. The Fluid Mosaic Model of the Structure of Cell Membranes. *Science* **1972**, *175*, 720−731.
(10) Simons, K.; Sampaio, J. L. Membrane Organization and Lipid Rafts. *Cold Spring Harbor Perspect. Biol.* **2011**, *3*, a004697.
(11) Lingwood, D.; Simons, K. Lipid Rafts as a Membrane-Organizing Principle. *Science* **2010**, *327*, 46−50.
(12) Van der Paal, J.; Hong, S.-H.; Yusupov, M.; Gaur, N.; Oh, J.-S.; Short, R. D.; Szili, E. J.; Bogaerts, A. How membrane lipids influence plasma delivery of reactive oxygen species into cells and subsequent dna damage: an experimental and computational study. *Phys. Chem. Chem. Phys.* **2019**, *21*, 19327−19341.
(13) Simons, K.; Ikonen, E. Functional Rafts in Cell Membranes. *Nature* **1997**, *387*, 569−572.
(14) Simons, K.; Toomre, D. Lipid Rafts and Signal Transduction. *Nat. Rev. Mol. Cell Biol.* **2000**, *1*, 31−39.
(15) Veatch, S. L.; Cicuta, P.; Sengupta, P.; Honerkamp-Smith, A.; Holowka, D.; Baird, B. Critical fluctuations in plasma membrane vesicles. *ACS Chem. Biol.* **2008**, *3*, 287−293.
(16) Rayermann, S. P.; Rayermann, G. E.; Cornell, C. E.; Merz, A. J.; Keller, S. L. Hallmarks of reversible separation of living, unperturbed cell membranes into two liquid phases. *Biophys. J.* **2017**, *113*, 2425−2432.
(17) King, C.; Sengupta, P.; Seo, A. Y.; Lippincott-Schwartz, J. ER membranes exhibit phase behavior at sites of organelle contact. *Proc. Natl. Acad. Sci. U. S. A.* **2020**, *117*, 7225−7234.
(18) Machta, B. B.; Papanikolaou, S.; Sethna, J. P.; Veatch, S. L. Minimal model of plasma membrane heterogeneity requires coupling cortical actin to criticality. *Biophys. J.* **2011**, *100*, 1668−1677.
(19) Miller, E. J.; Ratajczak, A. M.; Anthony, A. A.; Mottau, M.; Gonzalez, X. I. R.; Honerkamp-Smith, A. R. Divide and conquer: How phase separation contributes to lateral transport and organization of membrane proteins and lipids. *Chem. Phys. Lipids* **2020**, *233*, 104985.
(20) Arumugam, S.; Petrov, E. P.; Schwille, P. Cytoskeletal Pinning Controls Phase Separation in Multicomponent Lipid Membranes. *Biophys. J.* **2015**, *108*, 1104−1113.
(21) Aresta-Branco, F.; Cordeiro, A. M.; Marinho, H. S.; Cyrne, L.; Antunes, F.; de Almeida, R. F. M. Gel Domains in the Plasma Membrane of Saccharomyces Cerevisiae. *J. Biol. Chem.* **2011**, *286*, 5043−5054.
(22) Vecer, J.; Vesela, P.; Malinsky, J.; Herman, P. Sphingolipid Levels Crucially Modulate Lateral Microdomain Organization of Plasma Membrane in Living Yeast. *FEBS Lett.* **2014**, *588*, 443−449.
(23) Haluska, C. K.; Baptista, M. S.; Fernandes, A. U.; Schroder, A. P.; Marques, C. M.; Itri, R. Photo-activated Phase Separation in Giant Vesicles made from Different Lipid Mixtures. *Biochim. Biophys. Acta, Biomembr.* **2012**, *1818*, 666−672.
(24) Israelachvili, J. N.; Mitchell, D. J. A Model for the Packing of Lipids in Bilayer Membranes. *Biochim. Biophys. Acta, Biomembr.* **1975**, *389*, 13−19.
(25) Tsubone, T. M.; Junqueira, H. C.; Baptista, M. S.; Itri, R. Contrasting Roles of Oxidized Lipids in Modulating Membrane Microdomains. *Biochim. Biophys. Acta, Biomembr.* **2019**, *1861*, 660−669.
(26) Koynova, R.; Caffrey, M. Phases and Phase Transitions of the Phosphatidylcholines. *Biochim. Biophys. Acta, Rev. Biomembr.* **1998**, *1376*, 91−145.
(27) Jones, J. W.; Lue, L.; Saiani, A.; Tiddy, G. J. T. Density, DSC, X-ray and NMR measurements through the gel and lamellar phase transitions of 1-myristoyl-2-stearoyl-sn-glycero-3-phosphatidylcholine (MSPC) and 1-stearoyl-2-myristoyl-sn-glycero-3-phosphatidylcholine (SMPC): observation of slow relaxation processes and mechanisms of phase transitions. *Phys. Chem. Chem. Phys.* **2012**, *14*, 5452−5469.
(28) Cordeiro, R. M. Molecular Structure and Permeability at the Interface between Phase-Separated Membrane Domains. *J. Phys. Chem. B* **2018**, *122*, 6954−6965.
(29) Papahadjopoulos, D.; Jacobson, K.; Nir, S.; Isac, I. Phase Transitions in Phospholipid Vesicles: Fluorescence Polarization and Permeability Measurements Concerning the Effect of Temperature and Cholesterol. *Biochim. Biophys. Acta, Biomembr.* **1973**, *311*, 330−348.
(30) Heimburg, T. Lipid Ion Channels. *Biophys. Chem.* **2010**, *150*, 2−22.
(31) Wu, H. L.; Sheng, Y. J.; Tsao, H. K. Phase Behaviors and Membrane Properties of Model Liposomes: Temperature Effect. *J. Chem. Phys.* **2014**, *141*, 124906.
(32) Ghysels, A.; Kramer, A.; Venable, R. M.; Teague, W. E.; Lyman, E.; Gawrisch, K.; Pastor, R. W. Permeability of membranes in the liquid ordered and liquid disordered phases. *Nat. Commun.* **2019**, *10*, 5616.
(33) Yusupov, M.; Wende, K.; Kupsch, S.; Neyts, E. C.; Reuter, S.; Bogaerts, A. Effect of head group and lipid tail oxidation in the cell membrane revealed through integrated simulations and experiments. *Sci. Rep.* **2017**, *7*, 5761.
(34) Ayee, M. A. A.; LeMaster, E.; Shentu, T. P.; Singh, D. K.; Barbera, N.; Soni, D.; Tiruppathi, C.; Subbaiah, P. V.; Berdyshev, E.; Bronova, I.; Cho, M.; Akpa, B. S.; Levitan, I. Molecular-scale Biophysical Modulation of an Endothelial Membrane by Oxidized Phospholipid. *Biophys. J.* **2017**, *112*, 325−338.
(35) Oliveira, M. C.; Yusupov, M.; Bogaerts, A.; Cordeiro, R. M. How do Nitrated Lipids affect the Properties of Phospholipid Membranes? *Arch. Biochem. Biophys.* **2020**, *695*, 108548.
(36) Boonnoy, P.; Jarerattanachat, V.; Karttunen, M.; Wong-ekkabut, J. Bilayer Deformation, Pores, and Micellation Induced by Oxidized Lipids. *J. Phys. Chem. Lett.* **2015**, *6*, 4884−4888.
(37) Van der Paal, J.; Neyts, E. C.; Verlackt, C. C. W.; Bogarts, A. Effect of Lipid Peroxidation on Membrane Permeability of Cancer and Normal Cells Subjected to Oxidative Stress. *Chem. Sci.* **2016**, *7*, 489−498.
(38) Bacellar, I. O. L.; Tsubone, T. M.; Pavani, C.; Baptista, M. S. Photodynamic Efficiency: From Molecular Photochemistry to Cell Death. *Int. J. Mol. Sci.* **2015**, *16*, 20523−20559.
(39) Robert, E.; Darny, T.; Dozias, S.; Iseni, S.; Pouvesle, J. M. New insights on the propagation of pulsed atmospheric plasma streams: from single jet to multi jet arrays. *Phys. Plasmas* **2015**, *22*, 122007.
(40) Hirst, A. M.; Frame, F. M.; Arya, M.; Maitland, N. J.; O'Connell, D. Low temperature plasmas as emerging cancer therapeutics: the state of play and thoughts for the future. *Tumor Biol.* **2016**, *37*, 7021.
(41) Van Der Spoel, D.; Lindahl, E.; Hess, B.; Groenhof, G.; Mark, A. E.; Berendsen, H. J. C. GROMACS: Fast, Flexible, and Free. *J. Comput. Chem.* **2005**, *26*, 1701−1718.
(42) Oostenbrink, C.; Villa, A.; Mark, A. E.; Van Gunsteren, W. F. A Biomolecular Force Field Based on the Free Enthalpy of Hydration and Solvation: The GROMOS Force-field Parameter sets 53A5 and 53A6. *J. Comput. Chem.* **2004**, *25*, 1656−1676.
(43) Poger, D.; Mark, A. E. On the Validation of Molecular Dynamics Simulations of Saturated and cis-monounsaturated Phosphatidylcholine Lipid Bilayers: A Comparison with Experiment. *J. Chem. Theory Comput.* **2010**, *6*, 325−336.
(44) Neto, A. J. P.; Cordeiro, R. M. Molecular Simulations of the Effects of Phospholipid and Cholesterol Peroxidation on Lipid Membrane Properties. *Biochim. Biophys. Acta, Biomembr.* **2016**, *1858*, 2191−2198.
(45) Petrov, D.; Margreitter, C.; Grandits, M.; Oostenbrink, C.; Zagrovic, B. A systematic framework for molecular dynamics simulations of protein post-translational modifications. *PLoS Comput. Biol.* **2013**, *9*, e1003154.
(46) Oostenbrink, C.; Soares, T. A.; van der Vegt, N. F. A.; van Gunsteren, W. F. Validation of the 53A6 GROMOS force field. *Eur. Biophys. J.* **2005**, *34*, 273−284.

https://doi.org/10.1021/acs.jcim.1c00104
J. Chem. Inf. Model. 2021, 61, 2857−2868

(47) Martinez, L.; Andrade, R.; Birgin, E. G.; Martinez, J. M. Packmol: A package for Building Initial Configurations for Molecular Dynamics Simulations. *J. Comput. Chem.* **2009**, *30*, 2157−2164.
(48) Humphrey, W.; Dalke, A.; Schulten, K. VMD: Visual Molecular Dynamics. *J. Mol. Graphics* **1996**, *14*, 33−38.
(49) Gardner, H. W. Oxygen Radical Chemistry of Polyunsaturated Fatty Acids. *Free Radical Biol. Med.* **1989**, *7*, 65−86.
(50) Berendsen, H. J. C.; Postma, J. P. M.; van Gunsteren, W. F.; Hermans, J., Interaction Models for Water in Relation to Protein Hydration. In *Intermolecular Forces*; B. Pullman: Dordrecht, 1981; pp 331−342.
(51) Nose, S. A molecular-dynamics method for simulations in the canonical ensemble. *Mol. Phys.* **1984**, *52*, 255−268.
(52) Hoover, W. G. Canonical dynamics - equilibrium phase-space distributions. *Phys. Rev. A: At., Mol., Opt. Phys.* **1985**, *31*, 1695−1697.
(53) Parrinello, M.; Rahman, A. Polymorphic Transitions in Single-Crystals - A new molecular-dynamics method. *J. Appl. Phys.* **1981**, *52*, 7182−7190.
(54) Raudino, A.; Zuccarello, F.; La Rosa, C.; Buemi, G. Thermal expansion and compressibility coefficients of phospholipid vesicles: experimental determination and theoretical modeling. *J. Phys. Chem.* **1990**, *94*, 4217−4223.
(55) Rycroft, C. H. VORO++: A three-dimensional Voronoi cell library in C++. *Chaos* **2009**, *19*, 041111.
(56) Santos, D. E. S.; Pontes, F. J. S.; Lins, R. D.; Coutinho, K.; Soares, T. A. SuAVE: A Tool for Analyzing Curvature-Dependent Properties in Chemical Interfaces. *J. Chem. Inf. Model.* **2020**, *60*, 473−484.
(57) Camilo, C. R. S.; Ruggiero, J. R.; de Araujo, A. S. A Method for Detection of Permeation Events in Molecular Dynamics Simulations of Lipid Bilayers. *bioRxiv* **2021**, DOI: 10.1101/2021.01.20.427278.
(58) Runas, K. A.; Malmstadt, N. Low levels of lipid oxidation radically increase the passive permeability of lipid bilayers. *Soft Matter* **2015**, *11*, 499−505.
(59) Bennett, W. F. D.; Tieleman, D. P. Computer Simulations of Lipid Membrane Domains. *Biochim. Biophys. Acta, Biomembr.* **2013**, *1828*, 1765−1776.
(60) Carpenter, T. S.; López, C. A.; Neale, C.; Montour, C.; Ingólfsson, H. I.; Di Natale, F.; Lightstone, F. C.; Gnanakaran, S. Capturing Phase Behavior of Ternary Lipid Mixtures with a Refined Martini Coarse-Grained Force Field. *J. Chem. Theory Comput.* **2018**, *14*, 6050−6062.
(61) Kučerka, N.; Nieh, M.; Katsaras, J. Fluid Phase Lipid Areas and Bilayer Thicknesses of Commonly used Phosphatidylcholines as a Function of Temperature. *Biochim. Biophys. Acta, Biomembr.* **2011**, *1808*, 2761−2771.
(62) Weber, G.; Charitat, T.; Baptista, M. S.; Uchoa, A. F.; Pavani, C.; Junqueira, H. C.; Guo, Y.; Baulin, V. A.; Itri, R.; Marques, C. M.; Schroder, A. P. Lipid Oxidation Induces Structural Changes in Biomimetic Membranes. *Soft Matter* **2014**, *10*, 4241−4247.
(63) Beranova, L.; Cwiklik, L.; Jurkiewicz, P.; Hof, M.; Jungwirth, P. Oxidation Changes Physical Properties of Phospholipid Bilayers: Fluorescence Spectroscopy and Molecular Simulations. *Langmuir* **2010**, *26*, 6140−6144.
(64) Rosa, R. D.; Spinozzi, F.; Itri, R. Hydroperoxide and Carboxyl Groups Preferential Location in Oxidized Biomembranes Experimentally Determined by Small Angle X-Ray Scattering: Implications in Membrane. *Biochim. Biophys. Acta, Biomembr.* **2018**, *1860*, 2299−2307.
(65) Yesylevskyy, S.; Rivel, T.; Ramseyer, C. Curvature increases permeability of the plasma membrane for ions, water and the anti-cancer drugs cisplatin and gemcitabine. *Sci. Rep.* **2019**, *9*, 17214.
(66) Hanna, H.; Denzi, A.; Liberti, M.; André, F. M.; Mir, L. M. Electropermeabilization of Inner and Outer Cell Membranes with Microsecond Pulsed Electric Fields: Quantitative Study with Calcium Ions. *Sci. Rep.* **2017**, *7*, 1−14.
(67) Pasquet, L.; Chabot, S.; Bellard, E.; Rols, M. P.; Teissie, J.; Golzio, M. Noninvasive Gene Electrotransfer in Skin. *Hum. Gene Ther: Methods.* **2019**, *30*, 17−22.
(68) Bo, W.; Silkunas, M.; Mangalanathan, U.; Novickij, V.; Casciola, M.; Semenov, I.; Xiao, S.; Pakhomova, O. N.; Pakhomov, A. G. Probing Nanoelectroporation and Resealing of the Cell Membrane by the Entry of Ca2+ and Ba2+ Ions. *Int. J. Mol. Sci.* **2020**, *21*, 3386.
(69) Wiczew, D.; Szulc, N.; Tarek, M. On the Permeability of Cell Membranes Subjected to Lipid Oxidation. *bioRxiv* **2020**, DOI: 10.1101/2020.11.30.403345.
(70) Drummen, G. P. C.; Gadella, B. M.; Post, J. A.; Brouwers, J. F. Mass Spectrometric Characterization of the Oxidation of the Fluorescent Lipid Peroxidation Reporter Molecule C11-BODIPY581/591. *Free Radical Biol. Med.* **2004**, *36*, 1635−1644.
(71) Kaur, A.; Kolanowski, J. L.; New, E. J. Reversible Fluorescent Probes for Biological Redox States. *Angew. Chem., Int. Ed.* **2016**, *55*, 1602−1613.
(72) Michel, O.; Pakhomov, A. G.; Casciola, M.; Saczko, J.; Kulbacka, J.; Pakhomova, O. N. Electropermeabilization does not Correlate with Plasma Membrane Lipid Oxidation. *Bioelectrochemistry* **2020**, *132*, 107433.
(73) Schafer, L. V.; Marrink, S. J. Partitioning of Lipids at Domain Boundaries in Model Membranes. *Biophys. J.* **2010**, *99*, L91−L93.

https://doi.org/10.1021/acs.jcim.1c00104
J. Chem. Inf. Model. 2021, 61, 2857−2868